

# Near-infrared photonic crystals with higher-order bandgaps generated by two-photon photopolymerization

Martin Straub and Min Gu

Centre for Micro-Photonics, School of Biophysical Sciences and Electrical Engineering, Swinburne University of Technology, P.O. Box 218, Hawthorn, Victoria 3122, Australia

Received June 7, 2002

Three-dimensional photonic crystals with bandgaps of 1.5–2.3  $\mu\text{m}$  in wavelength and with gap/midgap ratios of as much as 18% were generated efficiently by two-photon photopolymerization in a liquid resin. From 0.5–1.1-mW femtosecond-pulsed 540-nm light, woodpile structures consisting of 40 layers of elliptically shaped rods spaced at 350–500 nm were fabricated by focusing with a 1.3-N.A. objective. The high degree of correlation in these structures allowed the suppression of infrared transmission by as much as 50% as well as the observation of higher-order bandgaps. We also investigated the decrease in the gap wavelength on reduction of layer spacing, in-plane rod spacing, and rod size. © 2002 Optical Society of America

OCIS codes: 220.4000, 160.5470, 300.6340, 130.0250, 140.7090.

Within the past decade three-dimensional (3-D) photonic crystals, which inhibit the propagation of light in any direction, have become the subject of intense research.<sup>1</sup> The 3-D confinement of light facilitates numerous applications such as waveguides with sharp bends, microlasers, and novel filter types. Photonic crystal microdevices may also be integrated in optical circuits. However, 3-D photonic crystal structures with a complete bandgap in the important near-infrared (NIR) region of the optical spectrum, for example, at the main telecommunication wavelengths of 850 nm and 1.3 and 1.55  $\mu\text{m}$  are not easily fabricated. Semiconductor technology facilitates NIR photonic crystals with large gap/midgap ratios,<sup>2–4</sup> as structural elements of the order of a few hundred nanometers and high dielectric contrasts are achieved routinely. However, as a surface technology it is more suitable for two-dimensional structures, whereas 3-D structures generally require sophisticated procedures such as multirun sputtering and etching. 3-D photonic crystals with submicrometer dimensions may also be achieved by self-organization of colloidal particles.<sup>5–7</sup> However, these techniques do not provide the flexibility of fabricating arbitrary structures with optimum bandgap properties and often contain many kinds of defect.

However, within the past few years two-photon photopolymerization has emerged as a novel microfabrication technique.<sup>8–12</sup> Because two-photon excitation confines chemical reactions to the center of the focus, arbitrarily shaped 3-D microstructures can be generated by use of comparatively cheap polymer materials. Complete 3-D bandgaps require filling of these polymerized microstructures by materials with high dielectric constant. However, the suppression of light propagation in certain directions could be achieved with a 15% dip in the optical transmission at  $\lambda = 4.0 \mu\text{m}$ ,<sup>13</sup> and the introduction of a defect layer yielded a sharp spike in the transmission inside the gap region.<sup>14</sup>

In this Letter we demonstrate that two-photon photopolymerization results in 3-D photonic crystals

with bandgaps in the NIR region and in particular at telecommunication wavelengths. We show that for woodpile structures consisting of stacks of ellipsoidal rods transmission at wavelengths from 1.5 to 2.3  $\mu\text{m}$  can be suppressed by as much as 50%. Depending on structural parameters, the gap can be shifted to any wavelength desired, as demonstrated by a decrease of its center of gravity from 1.9 to 1.6  $\mu\text{m}$  on reduction of layer spacing  $\delta z$  from 500 to 350 nm as well as by its strong in-plane rod-spacing dependence. A shift of the bandgap by approximately 10% to longer wavelengths is observed when the rod's cross section is doubled. As our structures show a high level of perfection, higher-order bandgaps are also observed.

The experimental setup is sketched in Fig. 1. Photonic bandgap structures were fabricated with a 5-W-pumped mode-locked Ti:sapphire laser (Mira 900-F; Coherent, Palo Alto, Calif.), which provided 140-fs pulses at a repetition rate of 76 MHz, combined

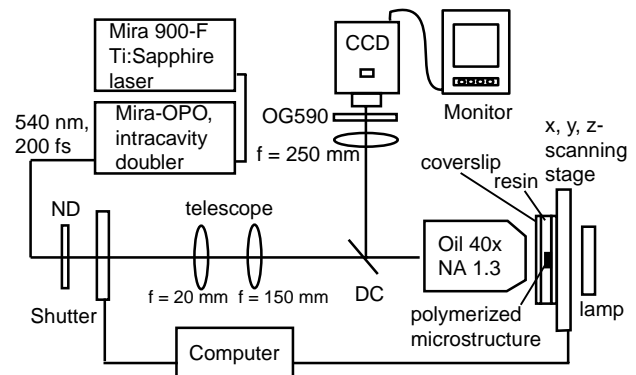


Fig. 1. Microfabrication setup. Ultrashort pulsed light ( $\lambda = 540 \text{ nm}$ ) initiates a polymerization reaction in the focus of a high-N.A. objective. Photonic crystals are generated by scanning of a preprogrammed path in the originally liquid resin. Transmitted light and sample fluorescence facilitate *in situ* monitoring of the process. OPO, optical parametric oscillator; OG590, orange glass filter; ND, neutral-density filter; DC, dichroic mirror; oil 40 $\times$ , N.A.-1.3 oil immersion objective.

with an optical parametric oscillator with an intracavity frequency doubler (Mira-OPO, Coherent; 1065–1265/545–625 nm). At a wavelength of 540 nm the laser beam of 0.5–1.1-mW power was focused onto the sample by a Zeiss Plan-Neofluar 40 $\times$  1.3-N.A. objective. We polymerized the rods by moving the sample relative to the focus at a speed of 30–90  $\mu\text{m/s}$ , using a computer-controlled 100  $\mu\text{m} \times 100 \mu\text{m} \times 20 \mu\text{m}$  piezoelectric stage (Physik Instrumente, Waldbronn, Germany). A 15- $\mu\text{m}$  frame was scanned about the structure to reduce imperfections caused by polymer shrinkage. Rectangular woodpile structures consisting of 40 layers of rods with 60–70- $\mu\text{m}$  lateral size and in-plane spacing  $\delta$  of 1.25–1.5  $\mu\text{m}$  were scanned within 30–60 min [see Fig. 2(a)]. SCR500 resin (Japan Synthetic Rubber Company; peak absorption in the UV, negligible absorption at 540 nm) containing urethane acrylate monomers and oligomers was used, as it provides high rigidity and stability of the polymerized structures. After the scanning the remaining liquid resin was washed out with ethanol. Infrared transmission spectra were measured with a Nicolet Nexus Fourier-transform infrared spectrometer (glow bar source, 200 scans at 4- $\text{cm}^{-1}$  resolution) combined with a Nicolet Continuum infrared microscope (32 $\times$  0.65-N.A. Reflexomat objective and condenser, MCT-A detector, aperture sizes chosen to be 35–45  $\mu\text{m} \times 45 \mu\text{m}$ ).

Woodpile structures provide many advantages for the fabrication process.<sup>15</sup> Straight rods can easily be stacked bottom up, yielding a comparatively stable arrangement. Even in low-index materials they exhibit large bandgaps for many rod sizes and shapes or in-plane spacings. Figures 2(b)–2(e) show electron microscope images of a 40-layer 60  $\mu\text{m} \times 60 \mu\text{m}$  structure scanned with 1.0 mW of power at 60  $\mu\text{m/s}$ . Subsequent layers were stacked at a layer spacing of 500 nm and an in-plane rod spacing of 1.5  $\mu\text{m}$ . Layers in this structure are well correlated, as can be seen from the shift of corresponding layers by half of an in-plane period [Figs. 2(c) and 2(d)]. However, polymer shrinkage and effects of the washout solvent can cause deviations of the rod shape from an ideal straight line, and stabilization of the structure by a frame is required. As the structure was not stabilized in the third dimension, it was contracted by 10–15% in its center. As can be seen from Fig. 2(e), the polymerized rods exhibit an ellipsoidal shape because the two-photon point-spread function is elongated in the axial direction owing to the finite aperture of the objective. At an excitation wavelength of 540 nm and a N.A. of 1.3 the two-photon excitation point-spread function should have full widths at half-maximum of 710 and 230 nm in the axial and the lateral directions, respectively.<sup>16</sup> Experimentally, rod sizes of 860 and 280 nm were observed; their ratio of 3.1 was in an excellent agreement with the prediction from theory. From the rod dimensions measured, it can directly be concluded that the polymerization threshold for these rods was at 60% of the maximum focal intensity.

Figure 3(a) shows the infrared spectra of the structure in Fig. 2 as well as an identical structure with

thinner rods that was produced with only half of the two-photon excitation density (0.5 mW, 30  $\mu\text{m/s}$ ). The Fourier-transform infrared spectra show a complex dependence of the optical transmission on the infrared wavelength. From 3.0 to 3.5  $\mu\text{m}$  in the transmission wavelength regime, polymer absorption bands are observed from C—H stretch vibrations. At

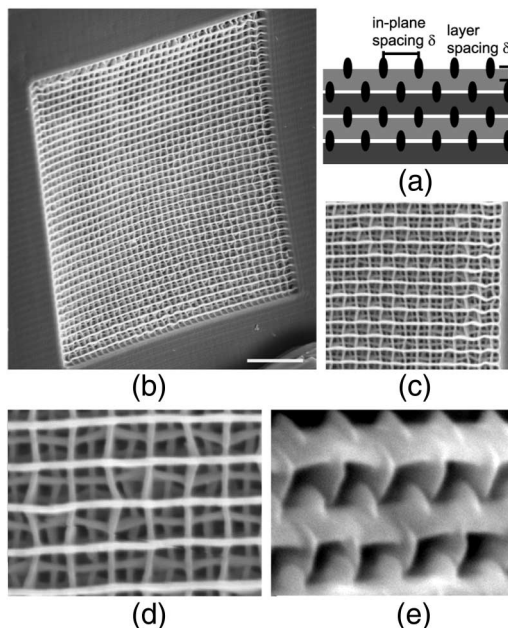


Fig. 2. Electron microscope images of a woodpile structure with 500-nm layer spacing and 1.5- $\mu\text{m}$  in-plane rod spacing. (a) Stacking arrangement: Subsequent layers lie at an angle of 90°, and corresponding layers are displaced by half of an in-plane period. (b) Complete 60  $\mu\text{m} \times 60 \mu\text{m}$  structure with the frame tilted by 40°. Scale bar, 10  $\mu\text{m}$ . (c) Top view, (d) magnified section, and (e) side view of the ellipsoidal rods with 860-nm axial and 280-nm lateral diameters.

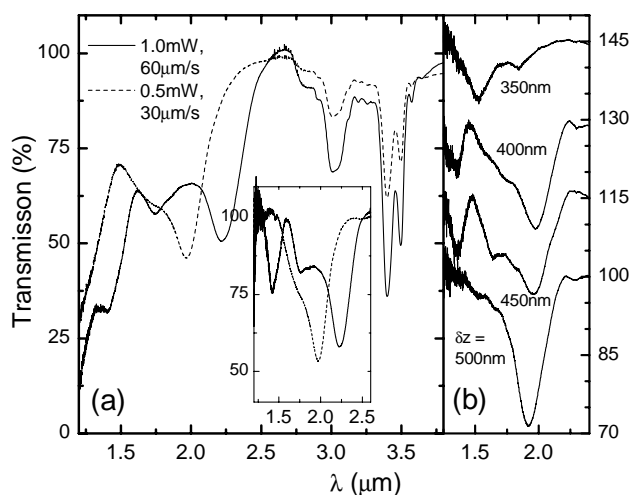


Fig. 3. (a) Infrared spectra of 40-layer woodpile structures with 500-nm layer spacing and a 1.5- $\mu\text{m}$  in-plane spacing. The main photonic bandgap shifts from 2.0 to 2.2  $\mu\text{m}$  when the rod size is increased. Note the smaller higher-order gap at 1.4  $\mu\text{m}$ . Inset, the baseline corrected gap shape. (b) Dependence of the photonic bandgap on the layer spacing (in-plane spacing, 1.25  $\mu\text{m}$ ).

shorter wavelengths the transmission drops to below 20% at a wavelength of 1  $\mu\text{m}$ , as light scattering by imperfections increases for wavelengths near the characteristic spacings of the structure. By contrast, the homogeneously polymerized resin is fully transparent below the wavelength of 3  $\mu\text{m}$ . Superimposed upon this drop are pronounced dips that are due to the existence of photonic bandgaps. The curve for the thinner-rod sample shows a sharp gap at 2.0  $\mu\text{m}$ , which is slightly asymmetrical with a shoulder toward shorter wavelengths. The inset in Fig. 3(a) presents the gap region after the baseline correction for the scattering effects. Transmission is suppressed by as much as 50%, and gap/midgap ratios are as large as 0.18. However, the width and the depth of the gap result from an average over angles of incidence of as much as 40° as a result of our 0.65-N.A. infrared objective. The thicker-rod structure exhibits more-complex bandgap features. The gap is located at 2.2  $\mu\text{m}$ , and the shoulder appears as an additional transmission minimum at 1.8  $\mu\text{m}$ . The change in the gap shape as the rod size varies may be explained by the different overlap between rods. From the depth of the polymer absorption peaks [Fig. 3(a)] it can be derived that the rod's cross section is smaller by a factor of 2 for the sample that has experienced lower exposure (dashed curve). This result is consistent with the shift in the gap position by 13% that is due to a corresponding change in the average dielectric constant of the structure.

Probably the most intriguing feature of the structure with thicker rods is the appearance of a higher-order gap at 1.4  $\mu\text{m}$ , which after the baseline correction reveals a quite respectable depth of 23%. Whereas in principle such higher-order gaps are a common feature of photonic crystals,<sup>1</sup> their observation requires the fabrication of structures with a high degree of perfection. This precision is ensured by the higher stability provided by the thicker rods, their stronger overlap, and the frame around the structure.

Figure 3(b) illustrates the dependence of the bandgap on layer spacing  $\delta z$  from 350 to 500 nm in steps of 50 nm. For this experiment a 65  $\mu\text{m} \times 70 \mu\text{m}$  woodpile structure with a rod cross section between those of Fig. 3(a) but with a 1.25- $\mu\text{m}$  in-plane rod spacing was scanned with 1.1 mW of power at 90  $\mu\text{m}/\text{s}$ . The bandgaps are located at shorter wavelengths, as the gap wavelength features a strong linear increase with the in-plane rod spacing  $\delta$  of as much as  $\Delta\lambda_{\text{gap}}/\Delta\delta = 1.0$  for  $1.0 \mu\text{m} \leq \delta \leq 2.0 \mu\text{m}$ . This dependence of wavelength on in-plane spacing is consistent with the results presented in Ref. 13 and appears to be a peculiarity of the woodpile structure. The gaps are less pronounced, probably because of the difference in the washout procedure, but for  $\delta z = 450$  nm and  $\delta z = 400$  nm sizable higher-order gaps are still observed with wavelengths near 1.35  $\mu\text{m}$ . On reduction of the layer spacing, the center of gravity of the gap gradually shifts from 1.9 to 1.6  $\mu\text{m}$ . On increasing overlap between the rods, a double-peaked shape develops. The shorter-wavelength part becomes increasingly more pronounced and,

eventually, dominates the spectrum at 1.5  $\mu\text{m}$  for the 350-nm stacking.

In conclusion, although all these gaps suppress IR transmission by only a maximum of 50% and still do not suppress it completely, these observations mark what we believe is the first evidence of photonic bandgaps in photopolymer microstructures in the NIR, in particular at telecommunication wavelengths. This is the first time of which we are aware that higher-order gaps have been observed in such samples. As the generation of structures at smaller layer spacings is impaired by the increasing overlap of polymerized rods, it is clearly desirable to introduce methods to sharpen the focus in the axial direction by appropriate superresolution techniques. As a consequence, high-quality photonic bandgap structures based on photopolymerized resins with sizable gaps in the NIR or even in the visible may soon become a reality.

The authors are grateful to Satoshi Kawata and Satoru Shoji, Osaka University, for kindly providing them with the SCR500 resin and acknowledge support from the Australian Research Council. M. Straub's e-mail address is mstraub@swin.edu.au.

## References

1. See J. Joannopoulos, R. Meade, and J. Winn, *Photonic Crystals* (Princeton U. Press, New York, 1995), and references therein.
2. J. G. Fleming and S.-Y. Lin, *Opt. Lett.* **24**, 49 (1999).
3. S. Noda, N. Yamamoto, H. Kobayashi, and M. Okano, *Appl. Phys. Lett.* **75**, 905 (1999).
4. J. Sabarinathan, P. Bhattacharya, D. Zhu, B. Kochman, and P.-C. Yu, *Appl. Phys. Lett.* **75**, 3024 (2001).
5. Y.-H. Ye, F. LeBlanc, A. Hache, and V.-V. Truong, *Appl. Phys. Lett.* **78**, 52 (2001).
6. G. Subramania, K. Constant, R. Biwas, M. M. Sigalas, and K.-M. Ho, *Appl. Phys. Lett.* **74**, 3933 (1999).
7. S. H. Foulger, S. Kotha, B. S. Sweryda-Krawiec, T. W. Baughman, and J. M. Ballato, *Opt. Lett.* **25**, 1300 (2000).
8. S. Maruo, O. Nakamura, and S. Kawata, *Opt. Lett.* **22**, 132 (1997).
9. S. Kawata, H. B. Sun, T. Tanaka, and K. Takada, *Nature* **412**, 697 (2001).
10. P. Galajda and P. Ormos, *Appl. Phys. Lett.* **78**, 249 (2001).
11. B. H. Cumpston, S. P. Ananthavel, S. Barlow, D. L. Dyer, J. E. Ehrlich, L. L. Erskine, A. A. Heikal, S. M. Kuebler, I.-Y. S. Lee, D. McCord-Maughon, J. Qin, H. Röckel, M. Rumi, X.-L. Wu, S. R. Marder, and J. W. Perry, *Nature* **398**, 51 (1999).
12. M. P. Joshi, H. E. Pudavar, P. N. Prasad, and B. A. Reinhardt, *Appl. Phys. Lett.* **74**, 170 (1999).
13. H. B. Sun, S. Matsuo, and H. Misawa, *Appl. Phys. Lett.* **74**, 786 (1999).
14. H. B. Sun, V. Mizeikis, Y. Xu, S. Joudkazis, J.-Y. Ye, S. Matsuo, and H. Misawa, *Appl. Phys. Lett.* **79**, 1 (2001).
15. R. Biwas, C. T. Chan, M. Sigalas, C. M. Soukoulis, and K. M. Ho, in *Photonic Band Gap Materials*, C. M. Soukoulis, ed., Vol. 315 of NATO ASI Series E (Kluwer Academic, Dordrecht, The Netherlands, 1996), pp. 23–40.
16. M. Gu, *Advanced Optical Imaging Theory* (Springer-Verlag, Berlin, 2000), p. 151.